British Journal of Pharmacology (2005) 144, 115–122
www.nature.com/bjp

Positron emission tomography using ^{18}F-labelled endothelin-1 reveals prevention of binding to cardiac receptors owing to tissue-specific clearance by ET_B receptors *in vivo*

*,[1]Peter Johnström, [2]Tim D. Fryer, [3]Hugh K. Richards, [2,3]Neil G. Harris, [2]Olivier Barret, [2]John C. Clark, [2,3]John D. Pickard & [1]Anthony P. Davenport

[1]Clinical Pharmacology Unit, University of Cambridge, Addenbrooke's Hospital, Cambridge; [2]Wolfson Brain Imaging Centre, University of Cambridge, Addenbrooke's Hospital, Cambridge and [3]Academic Neurosurgery Unit, University of Cambridge, Addenbrooke's Hospital, Cambridge

1 Our aim was to synthesise an ^{18}F analogue of endothelin-1 (ET-1), to dynamically image ET receptors *in vivo* by positron emission tomography (PET) and to elucidate the function of the ET_B subtype as a clearing receptor in organs expressing high densities including kidney and lung.

2 [^{18}F]-ET-1 was characterised *in vitro* and bound with a single subnanomolar affinity ($K_D = 0.43 \pm 0.05$ nM, $B_{max} = 27.8 \pm 2.1$ fmol mg^{-1} protein) to human left ventricle ($n = 4$).

3 The *in vivo* distribution of [^{18}F]-ET-1 in anaesthetised rats was measured using a dedicated small animal PET scanner (microPET) and *ex vivo* analysis.

4 Dynamic PET data demonstrated that high levels of radioligand accumulated rapidly in the lung, kidney and liver, consistent with receptor binding. The *in vivo* distribution correlated with the anatomical localisation of receptors detected *in vitro* using [^{125}I]-ET-1. However, the receptor density visualised in the heart was unexpectedly low compared with that predicted from the *in vitro* measurements.

5 [^{18}F]-ET-1 binding in lungs could not be displaced by the ET_B selective antagonist BQ788, in agreement with the proposed internalisation of ET-1 by ET_B receptors. In contrast, infusion of BQ788 prior to injecting [^{18}F]-ET-1 significantly reduce the amount of radioligand visualised in the ET_B rich lung and kidney by 85% ($P < 0.05$, $n = 3$) and 55% ($P < 0.05$, $n = 3$), respectively.

6 Under conditions of ET_B receptor blockade, the heart could be visualised by microPET imaging.

7 These results suggest that clearance by ET_B receptors in the lung and kidney prevents binding of ET-1 to receptors in the heart.

British Journal of Pharmacology (2005) **144,** 115–122. doi:10.1038/sj.bjp.0706064

Keywords: Endothelin; ET-1; positron emission tomography; PET; microPET; ^{18}F; *in vivo* imaging

Abbreviations: BQ3020, *N*-acetyl-Leu-Met-Asp-Lys-Glu-Ala-Val-Tyr-Phe-Ala-His-Leu-Asp-Ile-Ile-Trp; BQ788, *N-cis*-2,6-dimethylpiperidinocarbonyl-L-γ-methylleucyl-D-1-methoxycarbonyltryptophanyl-D-norleucine; DMSO, dimethyl sulphoxide; ET-1, endothelin-1; FR139317, (*R*)-2-[(*R*)-2-[(*S*)-2-[[1-(hexahydro-1H-azepinyl)]carbonyl]amino-4-methylpentanoyl]amino-3-[3-(1-methyl-1H-indoyl)]propionyl]amino-3-(2-pyridyl)propionic acid; PET, positron emission tomography; ROI, regions-of-interest

Introduction

The potent, vasoactive peptide endothelin-1 (ET-1) has been suggested to play a role in cardiovascular diseases including chronic heart failure, hypertension, atherosclerosis, cerebral vasospasm and pulmonary hypertension (Schiffrin *et al*., 1997; Miyauchi & Masaki, 1999; Kedzierski & Yanagisawa, 2001). The action of ET-1 is mediated by two receptor subtypes, ET_A and ET_B, that are widely expressed in human tissue (Davenport & Russell, 2001). In humans, ET-1 is thought to be continuously released from the endothelium, causing long-lasting vasoconstriction by stimulation of ET_A receptors present on the underlying smooth muscle and so contributing to the maintenance of normal vascular tone (Russell & Davenport, 1999). In contrast, ET-1 acting on ET_B receptors expressed by the endothelium causes vasodilatation through release of nitric oxide and prostacyclin (de Nucci *et al*., 1988) counterbalancing the vasoconstriction (Haynes & Webb, 1998). Furthermore, the ET receptor system is involved in the modulation of cell proliferation and apoptosis (Wu-Wong & Opgenorth, 2001). In chronically instrumented rats it has been demonstrated that exogenous administered ET-1 interacts with vascular ET receptors (Gardiner *et al*., 1993; 1994a, b).

Positron emission tomography (PET) is widely used to study transmitter systems *in vivo*. Recent developments in dedicated tomographs for laboratory animals have resulted in an improved spatial resolution of 1–2 mm (Chatziioannou, 2002; Lewis *et al*., 2002). These tomographs can delineate discrete

*Author for correspondence at: Clinical Pharmacology Unit, University of Cambridge, Addenbrooke's Centre for Clinical Investigation, Level 6, Box 110, Addenbrooke's Hospital, Cambridge CB2 2QQ, U.K.; E-mail: pjj20@medschl.cam.ac.uk
Advance online publication: 6 December 2004

organs and their larger substructures and consequently provide the means to study normal controls and rodent models of disease.

Two drug strategies are currently being pursued to prevent the unwanted actions of ET-1: ET_A selective or mixed ET_A/ET_B antagonists (Lüscher & Barton, 2000). However, the optimum pharmacological profile for the ET antagonists has not yet been fully clarified (Dupuis, 2000; Kalra *et al*., 2002; Ertl & Bauersachs, 2004). Reports in the literature have suggested that ET_B receptors in the lung and kidney might have an additional beneficial function clearing ET-1 from the circulation (Fukuroda *et al*., 1994). *In vitro* studies have shown that the ET-1/ET_B receptor complex is rapidly internalised following agonist stimulation and transported to the lysosomes for degradation, suggesting a mechanism for the clearance of ET-1 *via* this subtype (Bremnes *et al*., 2000; Oksche *et al*., 2000).

To test the hypothesis of tissue-specific removal of circulating peptide and further clarify the function of the ET_B subtype as a clearing receptor *in vivo*, our aim was to synthesise an ^{18}F analogue of ET-1 that retained high-affinity binding and use this ligand to dynamically image ET receptors in the presence and absence of the ET_B selective antagonist BQ788. Here we report for the first time the imaging of a vascular peptide receptor system using ^{18}F and microPET.

Methods

Animals

PET experiments were performed in male Sprague–Dawley rats (328 ± 14 g). All experiments were conducted in accordance with the United Kingdom Animal Scientific Procedures Act, 1986 and complied with guidelines of the local animal ethics committee. Rats were housed with free access to standard rat food and water prior to the experimental procedure.

In vitro *experiments*

Tissue preparation Human tissue was obtained with local ethical approval at the time of operation, snap frozen immediately in liquid nitrogen and stored at $-70^{\circ}C$ until use. Cryostat sections ($30\,\mu m$) were cut from the left ventricular wall from explanted hearts of recipient patients undergoing cardiac transplantation for dilated cardiomyopathy and normal renal tissue (containing cortex and medulla) obtained from the opposite pole to non-obstructing tumours following nephrectomy.

In vitro *binding characterisation of [^{18}F]-ET-1* [^{18}F]-ET-1 was characterised using ligand-binding assays as previously described (Davenport & Kuc, 2002). For association experiments, sections of human left ventricle were incubated with [^{18}F]-ET-1 (1 nM) for increasing time periods (0–120 min) and in saturation assays with increasing concentrations of [^{18}F]-ET-1 (5 pM–2.5 nM) for 90 min. For competition experiments, sections of kidney were incubated with a fixed concentration of [^{18}F]-ET-1. Inhibition of binding to ET_A or ET_B receptors was obtained by co-incubation with $1\,\mu M$ FR139317 (ET_A selective antagonist) and $1\,\mu M$ BQ3020 (ET_B selective agonist), respectively. Nonspecific binding in all assays was defined by co-incubating adjacent sections with unlabelled ET-1 ($1\,\mu M$). Specifically bound ligand was measured by gamma counting (Cobra II, PerkinElmer Life Sciences Ltd, Cambridge, U.K.) or by apposing the tissue to a storage phosphor imaging screen before analysis (Cyclone, PerkinElmer Life Sciences Ltd, Cambridge, U.K.). Binding was quantified using ^{18}F standard curves for gamma counting or co-exposing the standards with the tissue sections.

Animal preparation

Rats were anaesthetised with 3% isofluorane (Baker Norton, Bristol, U.K.) vaporised in N_2O/O_2 ($0.8/0.4\,l\,min^{-1}$) and maintained with 2% isofluorane. Body temperature was monitored and maintained in the normal range. A femoral vein was cannulated for administration of [^{18}F]-ET-1 and BQ788, and an artery cannulated for blood pressure monitoring. During PET scanning, anaesthesia was reduced to 1.5–2% isofluorane in N_2O/O_2 ($0.8/0.4\,l\,min^{-1}$).

MicroPET imaging

Study design Dynamic *in vivo* imaging of [^{18}F]-ET-1 binding to ET receptors in rat was studied using microPET. For control experiments using [^{18}F]-ET-1 alone, dynamic scans were performed for up to 2 h. To test the effect of ET_B receptor blockade, rats were pretreated with the ET_B antagonist BQ788 ($1\,mg\,kg^{-1}$) immediately prior to injection of [^{18}F]-ET-1 and imaged for 2 h. In one experiment, to test whether [^{18}F]-ET-1 binding could be displaced, BQ788 ($10\,mg\,kg^{-1}$) was infused 30 min after the administration of radioligand and the animal scanned for an additional 75 min. In one study, to obtain a whole-body distribution of ET-1, data were acquired in four separate bed positions, using 6×5 min time frames for each position, starting 20 min postinjection of [^{18}F]-ET-1.

MicroPET system Animals were imaged using a microPET P4 scanner (Tai *et al*., 2001) (Concorde Microsystems, Knoxville, U.S.A.). Rats were placed prone on the scanning bed and located in a purpose-built plastic stereotaxic frame. The computer controlled scanning bed was positioned so that the axial field of view (7.8 cm) encompassed the organs of interest.

Acquisition protocol [^{18}F]-ET-1 (7.8 ± 1.4 MBq) was administered to the rats as a bolus intravenous injection. A timing window of 10 ns was used in conjunction with an energy window of 250–750 keV to increase sensitivity. The data (except the whole-body scan) were initially acquired into the following time frames starting at the time of tracer administration: 10×0.5, 5×1, 15×2 and then in 5 min frames to the end of the experiment. Subsequently, the list-mode data in the first frame were binned into 6×2 s frames to provide sufficient sampling of the vena cava activity to permit normalisation of the scans for injected activity.

Image reconstruction All images were reconstructed using the 3D filtered backprojection algorithm (Kinahan & Rogers, 1989), adapted in-house to work with data from the microPET P4 scanner. Corrections for randoms, dead time and normalisation were applied to the data during reconstruction. Images

were reconstructed into $0.5 \times 0.5 \times 0.5\,mm^3$ voxels in an array of $200 \times 200 \times 151$ and a Hanning window cutoff at $0.8 \times$ Nyquist frequency was incorporated into the reconstruction filters.

Quantitative analysis of microPET data

Regions-of-interest (ROI) were delineated for the organs of interest using Analyze (Robb *et al*., 1989) (AnalyzeDirect Inc., Lenexa, U.S.A.) to construct time–activity curves. Consistently sized regions were used for all studies and were of sufficient size ($\geqslant 1.3$ ml) that quantification error due to the partial volume effect should not be significant for the resolution of the microPET. Data were corrected for decay and normalised for injected dose by the integral under the time–activity curve (up to the peak) for a ROI over the vena cava.

Ex vivo *tissue analysis*

At the end of scanning, animals were killed by intravenous injection of pentobarbitone and organs dissected, weighed and analysed for the amount of radioactivity. Cryostat cut sections were apposed to a storage phosphor imaging screen (Cyclone, PerkinElmer Life Sciences Ltd, Cambridge, U.K.). To compare the distribution of receptors detected by [^{18}F]-ET-1 with that obtained with the well-characterised *in vitro* ligand [^{125}I]-ET-1 tissue sections were stored at -70°C for a week (90 half-lives) to allow for the decay of ^{18}F. Sections were then re-incubated with a fixed concentration of [^{125}I]-ET-1 (0.1 nM) using the same conditions as for the saturation experiment above. Nonspecific binding was defined by co-incubating adjacent sections with unlabelled ET-1 (1 μM). Quantitative data in each experiment were obtained by co-exposing tissue with ^{18}F and ^{125}I standards respectively. To compare levels of ^{18}F and ^{125}I binding to tissue sections, quantitative data were normalised to values for the lung in each experiment.

Statistical analysis

Data are expressed as mean$\pm$s.e.m. The results from the association and saturation experiments were analysed using the KELL nonlinear iterative curve fitting suite of programmes (Biosoft, Cambridge, U.K.). The saturation data were fitted to a one- or two-site model using a nonlinear function. A two-site model was accepted only if it resulted in a significantly better fit as judged by an *F*-test ($P<0.05$). Mean values were compared using Student's *t*-test and differences were considered significant at $P<0.05$.

Peptides and radiolabelled compounds

ET-1 and BQ3020 were obtained from Peptide Institute Inc. (Osaka, Japan) and Neosystem (Strasbourg, France), respectively. BQ788 and FR 139317 were synthesised by Dr A.M. Doherty (Parke-Davis Pharmaceuticals Research Division, Ann Arbor, U.S.A.). [^{125}I]-ET-1 (2000 Ci mmol^{-1}) was obtained from Amersham Biosciences U.K. Ltd (Chalfont St Giles, U.K.). BQ788 for injection was dissolved in a small volume of DMSO before formulation in saline (2 mg ml^{-1}, 2% DMSO).

ET-1 was labelled with ^{18}F in the ε-amino group of Lys^9 by conjugation with the Bolton–Hunter type reagent *N*-succinimidyl 4-[^{18}F]fluorobenzoate (Johnström *et al*., 2002). Mean specific activity at injection was 182 ± 43 GBq μmol^{-1} and the radiochemical purity was $>95\%$.

Results

[^{18}F]-ET-1 in vitro *binding characteristics*

Binding of [^{18}F]-ET-1 to human left ventricle ($n=4$) was concentration-dependent and saturable (Table 1). A one-site model was preferred to a two-site model and the Hill slope (n_H) was close to unity. The binding was time-dependent with a half-time for association of 17 min and an association rate constant (k_{obs}) of 0.045 ± 0.004 min^{-1}.

Binding of [^{18}F]-ET-1 to human kidney ($n=4$) was partially inhibited by FR139317 (1 μM) and BQ3020 (1 μM), with a significant reduction in specific binding of $33.7\pm13.3\%$ ($P<0.05$) and $73.3\pm2.5\%$ ($P<0.05$) respectively.

MicroPET imaging

[^{18}F]-ET-1 in vivo *distribution and binding kinetics* In control rats, high uptake of radioactivity was found in the lung, liver, kidney and bladder. Low levels of uptake could be visualised in the thyroid, pituitary and salivary glands, whereas brain and bone showed no uptake (Figure 1a). Delineation of the heart was difficult in control rats (Figure 1a) whereas substructures in the kidney such as the glomeruli, cortex and inner medulla/papilla could be resolved in the reconstructed images from the microPET (Figure 4a).

The dynamic data showed a fast clearance of [^{18}F]-ET-1 from the circulation ($t_{1/2}=0.43$ min) with a concurrent accumulation of radioactivity in the lung and liver, which rapidly reached equilibrium (Figure 2). No reduction in the level of radioactivity was observed in the lung and liver during scanning up to 2 h (dynamic data shown for up to 1 h). In the kidney an initial equilibrium was reached with a later, slow increase in uptake of radioactivity after 20 min (Figure 2). Injection of [^{18}F]-ET-1 did not significantly alter blood pressure compared to baseline ($n=4$ animals).

Effect of ET_B receptor blockade Injection of the ET_B selective antagonist BQ788 (10 mg kg^{-1}) 30 min after radioligand administration could not displace binding in the lung (Figure 1b, dynamic data not shown). However, when BQ788 (1 mg kg^{-1}) was injected before administration of [^{18}F]-ET-1 a change in the distribution kinetics could be observed (Figures

Table 1 Dissociation constant (K_D), maximal density of receptors (B_{max}) and Hill coefficient (n_H) for [^{18}F]-ET-1 in human left ventricle

	K_D (nM)	B_{max} (fmol g^{-1} protein)	n_H
[^{18}F]-ET-1	0.43 ± 0.05	27.8 ± 2.1	0.95 ± 0.04
[^{125}I]-ET-1	0.354 ± 0.074	64.3 ± 9.8	0.97 ± 0.03

For comparison, data obtained by Molenaar *et al*. (1993) for [^{125}I]-ET-1 in human left ventricle is included.

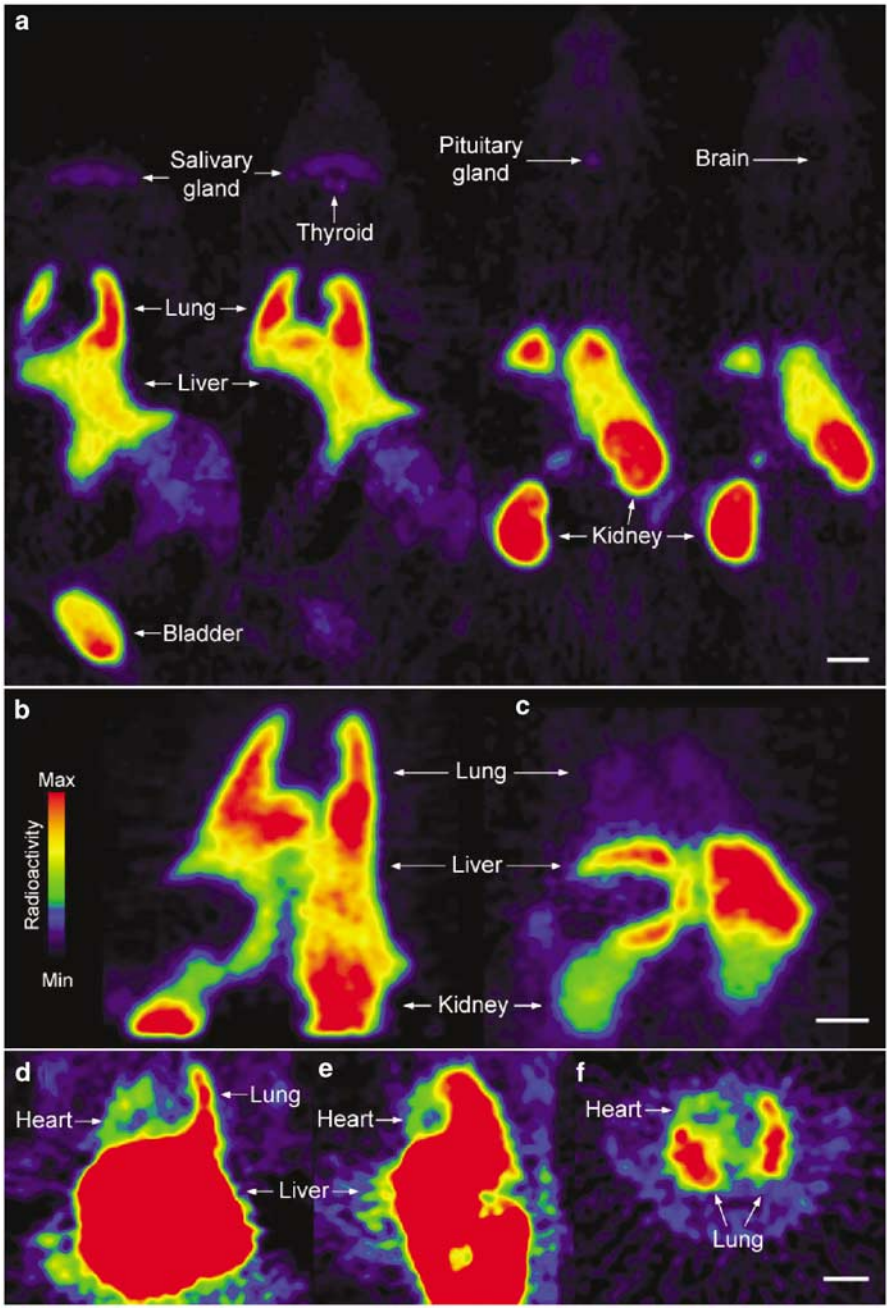

Figure 1 [^{18}F]-ET-1 microPET images: (a) whole-body distribution in four coronal planes; (b) distribution after injection of BQ788 revealing the lack of tracer displacement in the lung; (c) blockade of binding in the lung and kidney and increased uptake in the liver after preinjection of BQ788; visualisation of ET receptors in the heart after preinjection of BQ788 in coronal (d), sagittal (e) and transverse planes (f). Scale bars = 10 mm.

1c and 2). Significant reductions in uptake were observed in the lung and kidney, which at steady state were approximately 85% ($P<0.05$) and 55% ($P<0.05$), respectively (Figure 2). In contrast, liver showed a 40% increase in uptake, reaching significance after 1 h ($P<0.05$). A closer inspection of the initial uptake phase for the liver revealed a difference in the shape of the curve. In control rats equilibrium was reached within 2–3 min, whereas in the preblocked experiment a slower association was observed reaching steady state after 6–8 min (Figure 2e). When the animal was pretreated with BQ788, uptake in the heart wall could be visualised indicating binding to ET_A receptors (Figure 1d–f). As expected, preinjection of BQ788 caused a significant rise in blood pressure of 45% ($P=0.01$, $n=3$ animals) after infusion of the radioligand (Ishikawa *et al*., 1994). Vehicle for BQ788 (2% DMSO in saline) had no effect on [^{18}F]-ET-1 kinetics when infused alone.

[^{18}F]-ET-1 ex vivo *distribution*

Ex vivo analysis of the tissue corroborates the results obtained in the microPET, with lung the major uptake organ (Figure 3). After pretreatment with BQ788 the *ex vivo* data also showed a

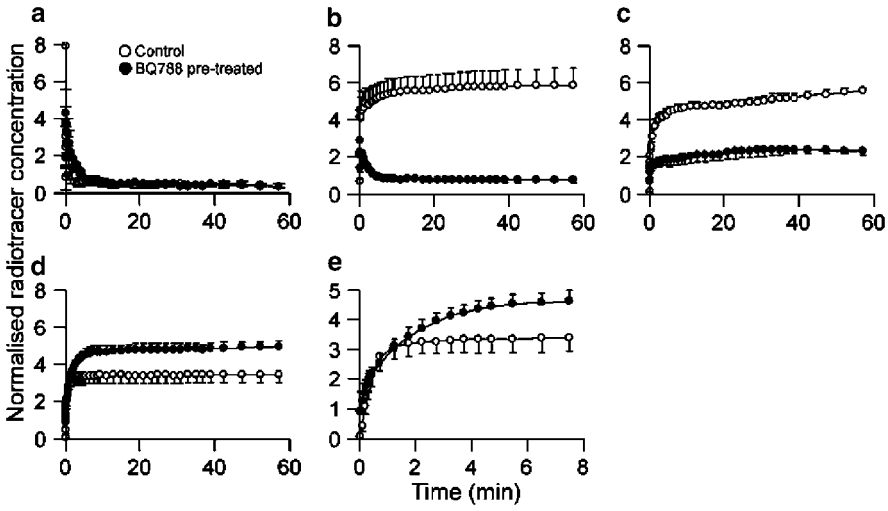

Figure 2 Time–activity curves for [^{18}F]-ET-1 in control ($n=3$) and BQ788 pretreated rats ($n=3$): (a) blood pool, (b) lung, (c) kidney, (d) liver and (e) liver (expanded time scale).

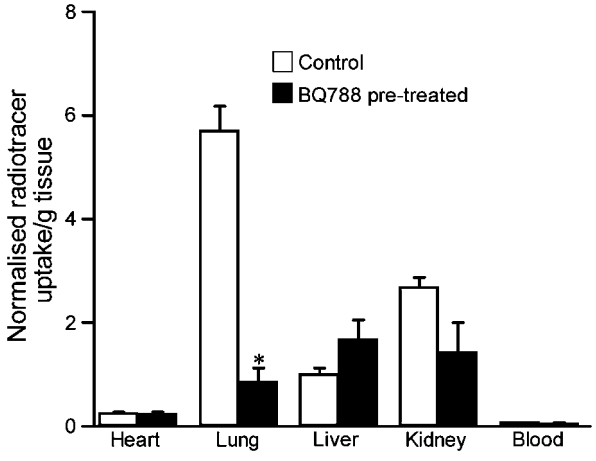

Figure 3 *Ex vivo* distribution of [^{18}F]-ET-1 in tissue for control ($n=3$) and BQ788 pretreated rats ($n=3$). Data were normalised for injected dose by the integral under the time–activity curve (up to the peak) using the dynamic PET data for a ROI over the vena cava. *$P<0.05$.

significant reduction in [^{18}F]-ET-1 uptake in the lung (85%, $P<0.05$). In the kidney and liver, the data followed the same trend as in the microPET studies, with a reduction in uptake for kidney (47%) and an increase in uptake in liver (67%), although these were not significant. No significant difference was observed in the heart between control and preblocked animals.

In vitro, the anatomical distribution of [^{125}I]-ET-1 matched the *ex vivo* distribution of [^{18}F]-ET-1 for all tissues except the brain and heart (Figure 4b). In the brain, the expected high density of ET receptors was visualised *in vitro* using [^{125}I]-ET-1, with complete absence of binding in the *ex vivo* study confirming the microPET observation that [^{18}F]-ET-1 does not cross the blood–brain barrier (Figures 4b and 5). Of more interest was our observation that the level of binding of [^{18}F]-ET-1 in the heart was much lower than would be predicted by the *in vitro* binding using [^{125}I]-ET-1 (Figures 4b and 5).

Distribution of [^{18}F]-ET-1 in lung sections revealed a more localised uptake in the BQ788 preblocked rats compared to the control experiments (Figure 6). The corresponding microPET images of the lung also suggest a more heterogeneous distribution of radioactivity.

Discussion

We have shown that [^{18}F]-ET-1 retains high-affinity binding with the expected single subnanomolar affinity comparable to values observed *in vitro* for [^{125}I]-ET-1 (Table 1) (Molenaar *et al*., 1993) and that binding was inhibited by ET_A or ET_B selective ligands to levels comparable to the ratio of ET_A/ET_B receptors densities previously reported for human kidney (ET_A: 35% and ET_B: 65%) (Karet *et al*., 1993). Furthermore, [^{18}F]-ET-1 can be used to visualise ET receptors with high resolution *in vivo* for at least 2 h using the new generation of small animal PET scanners. Although this study focused on larger organs, much smaller structures such as the thyroid and pituitary gland were easily delineated within the PET images, demonstrating that localised uptake in small structures below the notional resolution of the microPET can be resolved and imaged *in vivo*.

The distribution of receptors within organs visualised by [^{18}F]-ET-1 *in vivo* using microPET and *ex vivo* using autoradiography was directly comparable to the pattern revealed by *in vitro* labelling with [^{125}I]-ET-1, with two exceptions. As expected, [^{18}F]-ET-1 did not cross the blood–brain barrier and no binding was therefore detectable in brain following *in vivo* administration. Importantly, [^{18}F]-ET-1 unexpectedly labelled lower levels of receptors in the heart *in vivo* than predicted by the *in vitro* binding. Consequently, binding of [^{18}F]-ET-1 to heart could not be visualised by microPET imaging at any time during the time course of experiments (up to 2 h) in control animals. However, following pretreatment of the animals with the ET_B antagonist BQ788, the heart could be delineated in the images. No significant difference in heart uptake between control and pretreated rats was observed *ex vivo*, in accordance with [^{18}F]-ET-1 binding to ET_A receptors, the predominant subtype in the

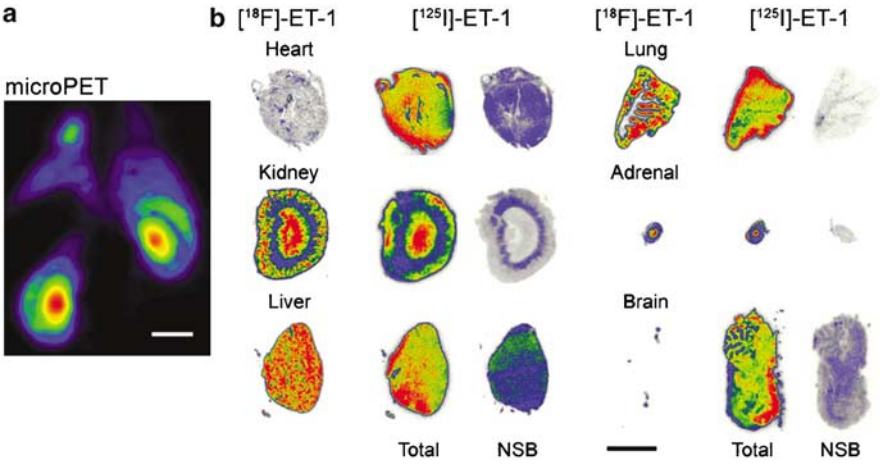

Figure 4 (a) [^{18}F]-ET-1 microPET image showing delineation of substructures in rat kidney. (b) Distribution within *ex vivo* tissue sections visualised using phosphor imaging after *in vivo* administration of [^{18}F]-ET-1 and *in vitro* incubation of the same tissue section with [^{125}I]-ET-1. Nonspecific binding (NSB) was determined using an adjacent section. The kidney distribution in the microPET image is similar to that seen in the *ex vivo* section but at a lower resolution. Scale bars = 10 mm.

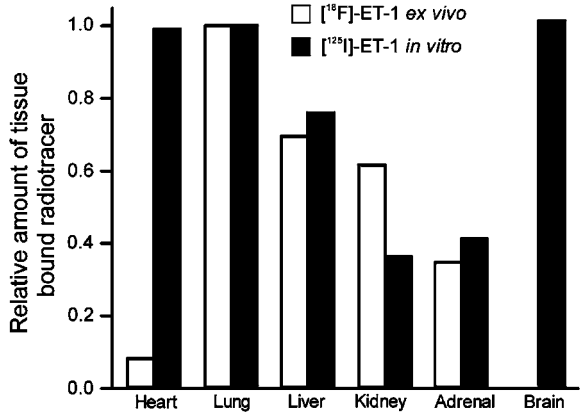

Figure 5 Comparison of the level of radioactivity bound to tissue sections from the *ex vivo* ([^{18}F]-ET-1) and the *in vitro* ([^{125}I]-ET-1) experiment. Quantitative data were normalised to values for the lung in each experiment.

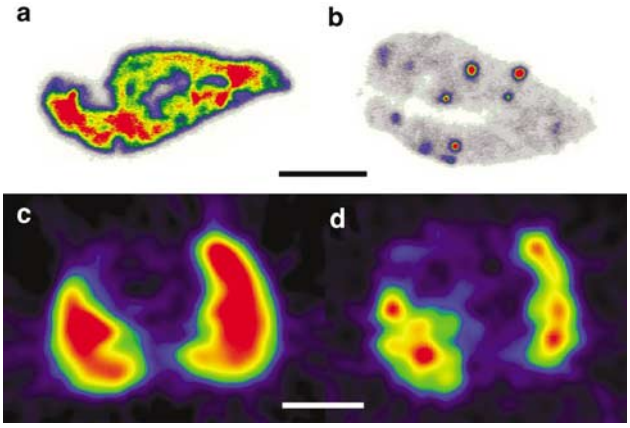

Figure 6 Distribution of [^{18}F]-ET-1 in the lung. *Ex vivo* tissue sections for (a) control and (b) BQ788 pretreated rat confirming blockade of nonvascular ET_B receptors. Scale bar = 5 mm. Transverse microPET images of the lungs revealing a more localised distribution in the BQ788 pretreated rat (d) compared to control (c). Scale bar = 10 mm.

heart (Peter & Davenport, 1996). In addition, the large decrease in lung uptake in the pretreated rats resulted in a reduction in intensity spillover from the lungs in the images, thus allowing delineation of the heart. In support of this hypothesis, we have previously synthesised an ET_A selective PET ligand [^{11}C]-PD156707 (Johnström *et al*., 2000) and successfully imaged the rat heart (unpublished results) and Aleksic *et al*. (2001), imaged receptors in the dog heart using [^{11}C]L-753,037, a mixed ET_A/ET_B receptor antagonist. Our results suggest that binding of circulating endogenous ligand to ET receptors in the heart might be prevented by the fast removal of ET-1 from the circulation by organs such as the lung and kidney.

Previous studies have suggested that the lung is an important site for the clearance of ET-1 from the circulation, mainly *via* the ET_B receptor (Fukuroda *et al*., 1994; Dupuis *et al*., 1996). We were able to follow this process dynamically in the rat using microPET. Our data show that [^{18}F]-ET-1 is rapidly cleared from the circulation within 2 min with a corresponding rapid accumulation in the lungs, consistent with receptor binding. The structure of ET-1, containing 21 amino acids linked by two disulphide bridges, is unique among mammalian bioactive peptides. Metabolic degradation of this peptide will result in abolition of receptor binding, for example, ET-1 will lose affinity to ET receptors with three orders of magnitude if the C-terminal Trp^{21} is removed (Kimura *et al*., 1988). Metabolism of [^{18}F]-ET-1 to shorter sequences would therefore result in radioactive fragments with little or no affinity for ET receptors. Furthermore, the absence of ^{18}F accumulation in bone indicates that the label did not undergo any significant defluorination over the time studied, suggesting that our kinetic data reflects binding of [^{18}F]-ET-1 to ET receptors in the lung.

In vitro studies have shown that the ET-1/receptor complex is rapidly internalised following agonist stimulation (Marsault *et al*., 1993; Chun *et al*., 1995; Bremnes *et al*., 2000; Oksche *et al*., 2000). The ET-1/ET_B complex is transported to the

lysosomes for degradation, suggesting a mechanism for the clearance of ET-1 *via* this subtype (Bremnes *et al*., 2000; Oksche *et al*., 2000). Our kinetic data *in vivo* support these findings: postinjection of the ET_B antagonist did not displace binding in the lung whereas pretreatment significantly reduced uptake, with levels comparable to previous observations using [^{125}I]-ET-1 (Fukuroda *et al*., 1994; Gibson *et al*., 1999). The *ex vivo* analysis of lung tissue from rats pretreated with BQ788 revealed a shift in the distribution of the radioactivity compared to the controls, with more prominent binding to the vasculature where the ET_A subtype predominates. The corresponding microPET images of the lung also suggest a more heterogeneous distribution indicative of binding to blood vessels in the lung.

In kidney, there was an initial fast accumulation of radioactivity that rapidly reached equilibrium within 10 min similar to the time–activity curve in the lung; the distribution *in vivo* was comparable to the pattern visualised *in vitro* in this and previous studies (Davenport *et al*., 1991) consistent with receptor binding. Treatment with the antagonist caused a significant reduction of uptake, in agreement with the ET_B receptor being the predominant subtype (Gellai *et al*., 1994), to levels comparable to those obtained previously with BQ788 (Fukuroda *et al*., 1994; Gibson *et al*., 1999). However, after $\sim$20 min, a slow increase in radioactivity was detected within the kidney. Although this could be the result of internalisation, since the time course is different to that of the lung and liver, an additional factor in the kidney may be accumulation of metabolites.

In control animals, the time–activity curves for liver showed a fast accumulation of radioactivity similar to that seen in the lung and kidney. However, under conditions of ET_B receptor blockade uptake increased in this organ. Interestingly, early dynamic data revealed an increase in time to reach equilibrium after pretreatment, suggesting blockade of ET_B receptor-mediated uptake. This is supported by the observation in isolated perfused liver that binding to ET_B receptors is the major route of clearance for ET-1 in single pass experiments (Dupuis *et al*., 1999). We cannot at this point conclude whether the later dynamic data, suggesting increased levels of binding to liver tissue, reflect increased levels of binding to ET_A receptors in lipocytes (Housset *et al*., 1993) or an increase in metabolic activity in liver cells (Gandhi *et al*., 1993). Further investigations are needed to completely elucidate the pharmacokinetics of [^{18}F]-ET-1 uptake in the liver; however, our initial data demonstrate the power of using PET in this type of study.

In conclusion, we have for the first time dynamically followed binding of ET-1 to ET receptors *in vivo* in the rat using microPET. Clearance of ET-1 was mediated by the ET_B receptor in the lung, kidney and to a certain extent by the liver. Furthermore, these results suggest that clearance by the ET_B receptor prevents binding of ET-1 to the heart. We hypothesise that this mechanism may be important in limiting the detrimental vasoconstrictor effect caused by upregulation of ET-1 in the vascular system associated with disease.

We thank Dr Adrian Carpenter, Mrs Rhoda Kuc and Mr Paul Burke for technical support and Dr Janet Maguire for helpful discussions. This work was supported by grants from the British Heart Foundation, the Medical Research Council Technology Foresight (U.K. Government) and for the microPET a JREI grant from HEFCE and Merck Sharp and Dohme, Ltd.

References

ALEKSIC, S., SZABO, Z., SCHEFFEL, U., RAVERT, H.T., MATHEWS, W.B., KERENYI, L., RAUSEO, P.A., GIBSON, R.E., BURNS, H.D. & DANNALS, R.F. (2001). In vivo labeling of endothelin receptors with [^{11}C]L-753,037: studies in mice and a dog. *J. Nucl. Med.,* **42,** 1274–1280.

BREMNES, T., PAASCHE, J.D., MEHLUM, A., SANDBERG, C., BREMNES, B. & ATTRAMADAL, H. (2000). Regulation and intracellular trafficking pathways of the endothelin receptors. *J. Biol. Chem.,* **275,** 17596–17604.

CHATZIIOANNOU, A.F. (2002). Molecular imaging of small animals with dedicated PET tomographs. *Eur. J. Nucl. Med. Mol. Imaging,* **29,** 98–114.

CHUN, M., LIN, H.Y., HENIS, Y.I. & LODISH, H.F. (1995). Endothelin-induced endocytosis of cell surface ET_A receptors. Endothelin remains intact and bound to the ET_A receptor. *J. Biol. Chem.,* **270,** 10855–10860.

DAVENPORT, A.P. & KUC, R.E. (2002). Radioligand binding assays and quantitative autoradiography of endothelin receptors. *Methods Mol. Biol.,* **206,** 45–70.

DAVENPORT, A.P., MORTON, A.J. & BROWN, M.J. (1991). Localization of endothelin-1 (ET-1), ET-2, and ET-3, mouse VIC, and sarafotoxin S6b binding sites in mammalian heart and kidney. *J. Cardiovasc. Pharmacol.,* **17** (Suppl 7), S152–S155.

DAVENPORT, A.P. & RUSSELL, F.D. (2001). Endothelin converting enzymes and endothelin receptor localisation in human tissues. In: *Endothelin and its Inhibitors,* ed. Warner, T.D., pp. 209–237. Berlin: Springer-Verlag.

DE NUCCI, G., THOMAS, R., D'ORLEANS-JUSTE, P., ANTUNES, E., WALDER, C., WARNER, T.D. & VANE, J.R. (1988). Pressor effects of circulating endothelin are limited by its removal in the pulmonary circulation and by the release of prostacyclin and endothelium-derived relaxing factor. *Proc. Natl. Acad. Sci. U.S.A.,* **85,** 9797–9800.

DUPUIS, J. (2000). Endothelin receptor antagonists and their developing role in cardiovascular therapeutics. *Can. J. Cardiol.,* **16,** 903–910.

DUPUIS, J., GORESKY, C.A. & FOURNIER, A. (1996). Pulmonary clearance of circulating endothelin-1 in dogs in vivo: exclusive role of ET_B receptors. *J. Appl. Physiol.,* **81,** 1510–1515.

DUPUIS, J., SCHWAB, A.J., SIMARD, A., CERNACEK, P., STEWART, D.J. & GORESKY, C.A. (1999). Kinetics of endothelin-1 binding in the dog liver microcirculation in vivo. *Am. J. Physiol.,* **277,** G905–G914.

ERTL, G. & BAUERSACHS, J. (2004). Endothelin receptor antagonists in heart failure: current status and future directions. *Drugs,* **64,** 1029–1040.

FUKURODA, T., FUJIKAWA, T., OZAKI, S., ISHIKAWA, K., YANO, M. & NISHIKIBE, M. (1994). Clearance of circulating endothelin-1 by ET_B receptors in rats. *Biochem. Biophys. Res. Commun.,* **199,** 1461–1465.

GANDHI, C.R., HARVEY, S.A. & OLSON, M.S. (1993). Hepatic effects of endothelin: metabolism of [^{125}I]endothelin-1 by liver-derived cells. *Arch. Biochem. Biophys.,* **305,** 38–46.

GARDINER, S.M., KEMP, P.A. & BENNETT, T. (1993). Regional haemodynamic responses to intravenous and intraarterial endothelin-1 and big endothelin-1 in conscious rats. *Br. J. Pharmacol.,* **110,** 1532–1536.

GARDINER, S.M., KEMP, P.A., MARCH, J.E. & BENNETT, T. (1994a). Effects of bosentan (Ro 47-0203), an ET_A-, ET_B-receptor antagonist, on regional haemodynamic responses to endothelins in conscious rats. *Br. J. Pharmacol.,* **112,** 823–830.

GARDINER, S.M., KEMP, P.A., MARCH, J.E., BENNETT, T., DAVENPORT, A.P. & EDVINSSON, L. (1994b). Effects of an ET_1-receptor antagonist, FR139317, on regional haemodynamic responses to endothelin-1 and [Ala^{11,15}]Ac-endothelin-1 (6–21) in conscious rats. *Br. J. Pharmacol.,* **112,** 477–486.

GELLAI, M., DEWOLF, R., PULLEN, M. & NAMBI, P. (1994). Distribution and functional role of renal ET receptor subtypes in normotensive and hypertensive rats. *Kidney Int.,* **46,** 1287–1294.

GIBSON, R.E., FIORAVANTI, C., FRANCIS, B. & BURNS, H.D. (1999). Radioiodinated endothelin-1: a radiotracer for imaging endothelin receptor distribution and occupancy. *Nucl. Med. Biol.,* **26,** 193–199.

HAYNES, W.G. & WEBB, D.J. (1998). Endothelin as a regulator of cardiovascular function in health and disease. *J. Hypertens.,* **16,** 1081–1098.

HOUSSET, C., ROCKEY, D.C. & BISSELL, D.M. (1993). Endothelin receptors in rat liver: lipocytes as a contractile target for endothelin 1. *Proc. Natl. Acad. Sci. U.S.A.,* **90,** 9266–9270.

ISHIKAWA, K., IHARA, M., NOGUCHI, K., MASE, T., MINO, N., SAEKI, T., FUKURODA, T., FUKAMI, T., OZAKI, S., NAGASE, T., NISHIKIBE, M. & YANO, M. (1994). Biochemical and pharmacological profile of a potent and selective endothelin B-receptor antagonist, BQ-788. *Proc. Natl. Acad. Sci. U.S.A.,* **91,** 4892–4896.

JOHNSTRÖM, P., AIGBIRHIO, F.I., CLARK, J.C., DOWNEY, S.P.M.J., PICKARD, J.D. & DAVENPORT, A.P. (2000). Syntheses of the first endothelin-A- and -B-selective radioligands for positron emission tomography. *J. Cardiovasc. Pharmacol.,* **36** (Suppl 1), S58–S60.

JOHNSTRÖM, P., HARRIS, N.G., FRYER, T.D., BARRET, O., CLARK, J.C., PICKARD, J.D. & DAVENPORT, A.P. (2002). ^{18}F-Endothelin-1, a positron emission tomography (PET) radioligand for the endothelin receptor system: radiosynthesis and *in vivo* imaging using microPET. *Clin. Sci.,* **103** (Suppl 48), 4S–8S.

KALRA, P.R., MOON, J.C.C. & COATS, A.J.S. (2002). Do results of the ENABLE (endothelin antagonist bosentan for lowering cardiac events in heart failure) study spell the end for non-selective endothelin antagonism in heart failure? *Int. J. Cardiol.,* **85,** 195–197.

KARET, F.E., KUC, R.E. & DAVENPORT, A.P. (1993). Novel ligands BQ123 and BQ3020 characterize endothelin receptor subtypes ET_A and ET_B in human kidney. *Kidney Int.,* **44,** 36–42.

KEDZIERSKI, R.M. & YANAGISAWA, M. (2001). Endothelin system: the double-edged sword in health and disease. *Annu. Rev. Pharmacol. Toxicol.,* **41,** 851–876.

KIMURA, S., KASUYA, Y., SAWAMURA, T., SHINMI, O., SUGITA, Y., YANAGISAWA, M., GOTO, K. & MASAKI, T. (1988). Structure–activity relationships of endothelin: importance of the C-terminal moiety. *Biochem. Biophys. Res. Commun.,* **156,** 1182–1186.

KINAHAN, P.E. & ROGERS, J.G. (1989). Analytic 3D image-reconstruction using all detected events. *IEEE Trans. Nucl. Sci.,* **36,** 964–968.

LEWIS, J.S., ACHILEFU, S., GARBOW, J.R., LAFOREST, R. & WELCH, M.J. (2002). Small animal imaging. Current technology and perspectives for oncological imaging. *Eur. J. Cancer,* **38,** 2173–2188.

LÜSCHER, T.F. & BARTON, M. (2000). Endothelins and endothelin receptor antagonists: therapeutic considerations for a novel class of cardiovascular drugs. *Circulation,* **102,** 2434–2440.

MARSAULT, R., FEOLDE, E. & FRELIN, C. (1993). Receptor externalization determines sustained contractile responses to endothelin-1 in the rat aorta. *Am. J. Physiol.,* **264,** C687–C693.

MIYAUCHI, T. & MASAKI, T. (1999). Pathophysiology of endothelin in the cardiovascular system. *Annu. Rev. Physiol.,* **61,** 391–415.

MOLENAAR, P., O'REILLY, G., SHARKEY, A., KUC, R.E., HARDING, D.P., PLUMPTON, C., GRESHAM, G.A. & DAVENPORT, A.P. (1993). Characterization and localization of endothelin receptor subtypes in the human atrioventricular conducting system and myocardium. *Circ. Res.,* **72,** 526–538.

OKSCHE, A., BOESE, G., HORSTMEYER, A., FURKERT, J., BEYERMANN, M., BIENERT, M. & ROSENTHAL, W. (2000). Late endosomal/lysosomal targeting and lack of recycling of the ligand-occupied endothelin B receptor. *Mol. Pharmacol.,* **57,** 1104–1113.

PETER, M.G. & DAVENPORT, A.P. (1996). Characterization of the endothelin receptor selective agonist, BQ3020 and antagonists BQ123, FR139317, BQ788, 50235, Ro462005 and bosentan in the heart. *Br. J. Pharmacol.,* **117,** 455–462.

ROBB, R.A., HANSON, D.P., KARWOSKI, R.A., LARSON, A.G., WORKMAN, E.L. & STACY, M.C. (1989). Analyze: a comprehensive, operator-interactive software package for multidimensional medical image display and analysis. *Comput. Med. Imaging Graph,* **13,** 433–454.

RUSSELL, F.D. & DAVENPORT, A.P. (1999). Secretory pathways in endothelin synthesis. *Br. J. Pharmacol.,* **126,** 391–398.

SCHIFFRIN, E.L., INTENGAN, H.D., THIBAULT, G. & TOUYZ, R.M. (1997). Clinical significance of endothelin in cardiovascular disease. *Curr. Opin. Cardiol.,* **12,** 354–367.

TAI, Y.C., CHATZIIOANNOU, A., SIEGEL, S., YOUNG, J., NEWPORT, D., GOBLE, R.N., NUTT, R.E. & CHERRY, S.R. (2001). Performance evaluation of the microPET P4: a PET system dedicated to animal imaging. *Phys. Med. Biol.,* **46,** 1845–1862.

WU-WONG, J.R. & OPGENORTH, T.J. (2001). The roles of endothelins in proliferations, apoptosis and angiogenesis. In: *Endothelin and its Inhibitors,* ed. Warner, T.D., pp. 299–322. Berlin: Springer-Verlag.

(Received September 30, 2004
Accepted October 20, 2004)